Electronic structure of intermetallic LiTl and NaTl

P. C. Schmidt
Physikalische Chemie III, Institut für Physikalische Chemie, Petersenstrasse 20, D-6100 Darmstadt, West Germany
(Received 17 September 1984)

The charge distribution, Knight shift K_s, and total energy E of intermetallic LiTl and NaTl have been calculated by the relativistic augmented-plane-wave method. For the $B32$-phase NaTl it is found that the valence-electron bands are separated by a band gap. The lower valence bands are built up by the $6s$ electrons of Tl forming covalent s-like bands within the diamondlike Tl sublattice. These $6s$ bands give a negative contribution to K_s(Tl) of -0.52% due to the exchange polarization effect. The valence bands above the $6s$ bands are sp bands of predominantly metallic character. In the $B2$-phase LiTl all valence bands overlap and the covalent character of the lower valence bands is much less pronounced than in NaTl. Theoretically the following values for K_s are found: $K_s(Li\mathrm{Tl}) = 0.003\%$, $K_s(\mathrm{Li}Tl) = 1.0\%$, $K_s(Na\mathrm{Tl}) = 0.002\%$, and $K_s(\mathrm{Na}Tl) = -0.14\%$. The agreement with the experimental results is good besides $K_s(\mathrm{Na}Tl)$ [K_s(expt., $\mathrm{Na}Tl) = -0.96\%$]. From the shape of the electron bands near the Fermi surface one could conclude that the difference between K_s(theor., $\mathrm{Na}Tl$) and K_s(expt. $\mathrm{Na}Tl$) is caused by a diamagnetic contribution to K_s. To obtain some insight in the stability of Zintl phases ($B32$ structure), the energy difference $\Delta E = E(B2) - E(B32)$ is calculated. One obtains $\Delta E(\mathrm{LiTl}) = -0.15$ eV per atom and $\Delta E(\mathrm{NaTl}) = +0.005$ eV per atom. The physical mechanisms which lead to the different signs in ΔE are discussed.

I. INTRODUCTION

Intermetallic NaTl is the prototype of the Zintl phases ($B32$ structure),[1] whereas LiTl crystallizes in the CsCl-type structure ($B2$ structure). In a simple picture both structures, $B2$ and $B32$, are superstructures of the bcc lattice (Fig. 1). Compared to most intermetallic phases the Zintl phases have some unusual physical properties: (a) The nearest neighbors are four like and four unlike atoms, whereas for most structures (e.g., the $B2$ structure) the nearest neighbors are unlike atoms; (b) the chemical shift of the NMR signal (Knight shift K_s) is distinctly smaller than the corresponding shift in the pure metals or in "normal" alloys;[2,3] e.g., $K_s(^{205}\mathrm{Tl})$ is equal to -0.96% in NaTl,[2] 1.66% in Tl metal,[4] and 1.2% in LiTl;[5] and (c) the chemical bond in Zintl phases is described as metallic, covalent and ionic.[6]

To get some insight in the unusual electronic properties of the Zintl phases, we have compared the electronic structures of the Zintl phase NaTl and the $B2$-phase LiTl. LiTl and NaTl have been shown for three reasons. Firstly, both are alkali-thallium phases. Secondly, for both phases the Knight shifts are very different (see above). Thirdly, the $B2$ and the $B32$ structures are both superstructures of the bcc structure.

There are several ways to calculate the difference in the ordering energies for the $B2$- and the $B32$-type structures. The comparison of the $B2$- and $B32$-type structure has been performed in the literature using the same neighboring distances for both lattices. From the pseudopotential method[7,8] one obtains differences in the band-energy values. However, significant differences could not be found by comparing $B2$- and $B32$-type compounds.[8] McNeil *et al.*[8] have found that Zintl phases are only found for those compounds AB for which the sizes of A

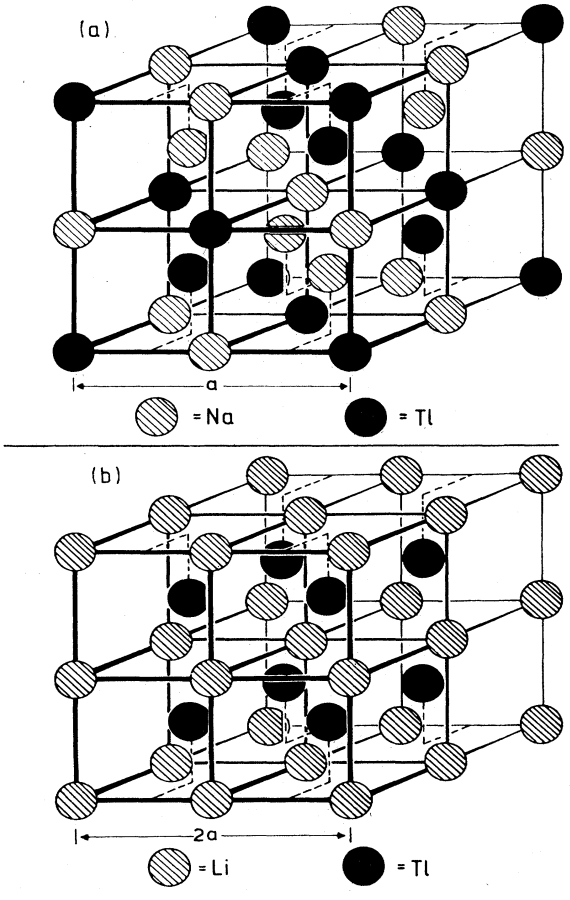

FIG. 1. Unit cells for NaTl and LiTl. a is the lattice constant.

and B are nearly the same.

In this paper we discuss the influence of the band structure as well as the influence of the size of the atoms on the lattice energy for the compounds LiTl and NaTl. For this purpose we have also calculated the band structure of LiTl for a hypothetical $B32$-phase LiTl, with name LiTl($B32$). In an analogous manner the band structure of hypothetical NaTl($B2$) has been studied. The calculation for both structures for the same compound have been performed for lattice constants $a_{B32}=2a_{B2}$. Then the neighboring distances of the atoms are the same for both lattices, and both lattices only differ in the arrangement of the atoms on the lattice sites; see Fig. 1. For this case the difference in the ordering energy $\Delta E=E(B2)-E(B32)$ can be estimated very easily by calculating the difference in the sum of the one-electron energies using the same potential around the atoms.[9,10] ΔE is also calculated from the energy expressions, which one gets from the local-density approach.[11,12]

From Fig. 1 it can be seen that in the Zintl-phase NaTl the Na and the Tl atoms form sublattices of the diamond type. In the valence-state picture the covalent bonds in diamond are formed by sp^3 hybrids. Therefore it is assumed that similar bonds are built by the diamond-type sublattice of the Tl atoms in NaTl.[1,6] Since the tetravalent elements crystallize in the diamond structure, it is assumed that the trivalent Tl receives the 4th electron from the Na atom. Therefore, a large charge transfer should take place in NaTl from Na to Tl. An indication for this charge transfer gives the Knight shift, which on one hand is nearly zero at the Na site[13] (that is, one finds roughly the NMR signal of Na^+), and which is on the other hand negative at the Tl site, indicating pure p conduction bands.[14] In the present paper the charge distribution and the character of the chemical bond in NaTl and LiTl are studied by comparing the amount of charge in the different atomic region of the solid and by plotting contour maps of the charge density for the electron states of these phases.

In addition to the energy states and the charge distribution, we have studied the Knight shift K_s. The contributions to K_s are caused by the spin (direct[15] and exchange polarization[14,16] terms) and by angular momentum (diamagnetic[17] and orbital[18] effects). In simple metals and alloys with sp-like wave functions the direct contribution caused by the Pauli paramagnetism[15] is the main part of K_s. It is expected that this also holds for the Knight shift in LiTl. In NaTl the situation is much more complicated. Firstly, NaTl is diamagnetic,[19] and we expect, that diamagnetic Landau contributions to K_s are also important.[3] Secondly, calculations of the hyperfine-coupling constant for the Tl atom have shown[20] that the contribution of the exchange polarization of the $6s$ electrons by the $6p$ electron is large. Therefore, the exchange polarization of the inner valence bands in NaTl should give a distinct contribution to K_s. Thirdly, since the conduction bands are expected to be sp-hybrid bands, the direct contribution to K_s must also be considered. In the present paper only the contributions caused by the spin, including the spin-orbit coupling, could be investigated but not the diamagnetic Landau contribution.

The calculations have been carried out by means of a relativistic augmented-plane-wave (RAPW) technique[21] using the muffin-tin approximation for the construction of the crystal potential and using the ansatz of the local electron-density theory for the total energy.[11,22–24] Since a large amount of computer time is needed for a full self-consistent RAPW calculation, the self-consistent muffin-tin potential was calculated by the simpler scalar RAPW (SRAPW) method,[25] for which the spin-orbit coupling is neglected and where the spin has a good quantum number. Therefore in the following we mean by RAPW a full relativistic augmented-plane-wave calculation[21] using a self-consistent potential obtained from SRAPW calculations. In the next section the formulas for the total energy and the Knight shift are briefly outlined and details for the used numerical procedure are given. In Sec. III the results of the band-structure calculations for LiTl and NaTl are presented, and in the last section these results are discussed in view of the questions of the electronic properties introduced above.

II. THEORY

A. Total energy

The total energy is calculated on the basis of the relativistic version of the local-density-functional approach and on the basis of the muffin-tin model. The total energy of a solid with frozen nuclei is given by[11,22–24]

$$E=T+U+E_{\rm xc}+E_{KK}\ , \tag{1}$$

$$T=\sum_{i=1}^{N}\langle\psi_i^*(-ic\boldsymbol{\gamma}\cdot\boldsymbol{\nabla}+\tfrac{1}{2}c^2)\psi_i\rangle\ , \tag{2}$$

$$U=-2\sum_s\int\frac{Z_s\rho(\mathbf{r})}{|\mathbf{r}-\mathbf{r}_s|}d\tau+\int\int\frac{\rho(\mathbf{r})\rho(\mathbf{r}')}{|\mathbf{r}-\mathbf{r}'|}d\tau\,d\tau'\ , \tag{3}$$

$$\rho(\mathbf{r})=\sum_{i=1}^{N}|\psi_i(\mathbf{r})|^2\ , \tag{4}$$

$$E_{KK}=\sum_{\substack{s,s'\\ s\neq s'}}\frac{Z_sZ_{s'}}{|\mathbf{r}_s-\mathbf{r}_{s'}|}\ . \tag{5}$$

N is the number of electrons and Z_s is the nuclear charge. The wave functions (4-spinors) ψ_i are solutions of the one-electron Dirac equations

$$[-ic\boldsymbol{\alpha}\cdot\boldsymbol{\nabla}+\tfrac{1}{2}\beta c^2+V(\mathbf{r})]\psi_i=\epsilon_i\psi_i\ , \tag{6}$$

$$V(\mathbf{r})=\frac{\delta U}{\delta\rho}+\frac{\delta E_{\rm xc}}{\delta\rho}=\frac{\delta U}{\delta\rho}+\mu_{\rm xc}\ . \tag{7}$$

There are numerous approaches to the exchange-correlation energy $E_{\rm xc}$ and potential $\mu_{\rm xc}$ in the literature.[12,26–29] In the present work we have used the relativistic exchange energy proposed by MacDonald and Vosko[24] and the correlation energy suggested by Vosko *et al.*[29] for all calculations.

The potential $V(\mathbf{r})$ [Eq. (7)] and the electrostatic energy U [Eq. (3)] are calculated on the basis of the muffin-tin

approximation. The volume of the unit cell ω is separated in the volume of nonoverlapping atomic spheres ω_s, s=Li, Na, and Tl, and the volume between the spheres ω'. The following three approximations are made for calculating $V(\mathbf{r})$ and U. (a) The electron density in ω' can be approximated by a constant

$$\rho_0 = Q'/\omega' , \tag{8}$$

where Q' is the electron charge in units of $-e$ within the volume ω'. (b) The electron charge density inside the muffin-tin spheres $\rho(\mathbf{r})$ can be replaced by the spherical mean

$$\rho_s(r) = \frac{1}{4\pi} \int\int \rho(\mathbf{r}) d\varphi \, d\cos\vartheta . \tag{9}$$

(c) The distant terms are calculated by a procedure proposed by Slater and de Cicco.[30]

Then one obtains for the potential inside the muffin-tin s with radius R_s

$$V_s(r) = V_s^H + \phi_s + \mu_{xc}(\rho_s) \tag{10}$$

where V_s^H is the local Hartree potential

$$V_s^H(r) = -2\frac{Z_s}{r} + 8\pi \left[\frac{1}{r} \int_0^r \rho_s(r')(r')^2 dr' + \int_r^{R_s} \rho_s(r') r' \, dr' \right] . \tag{11}$$

and ϕ_s is equal to the distant term

$$\phi_s = -3\rho_0 \frac{\omega_s}{R_s} - 2 \sum_{s'=1}^{\nu_s} E_{s'} M_{ss'} , \tag{12}$$

where

$$E_s = Z_s - Q_s + \rho_0 \omega_s , \tag{13}$$

$$Q_s = 4\pi \int_0^{R_s} \rho_s(r) r^2 \, dr , \tag{14}$$

and the values for $M_{ss'}$ are given in Table I. The summation in Eq. (12) is taken over all different kinds of muffin tins within the unit cell; the number of atoms in the unit cell is $\sum \nu_s = m$.

Outside the muffin tins the potential is a constant V_0:

$$V_0 = \phi_0 + \mu_{xc}(\rho_0) , \tag{15}$$

TABLE I. Values $aM_{ss'}$ in atomic units (a_0 Ry) for the CsCl- and the NaTl-type structures. a is the lattice constant; see Fig. 1. The values are calculated by Hund's method (Ref. 31), taking the electrostatic potential from Hajj (Ref. 32).

	CsCl	NaTl
$s=s'$	−2.837 297	−5.386 791
$s\neq s'$	−0.801 936	−1.891 66

$$\phi_0 = \frac{2}{\omega'} \left[\sum_{s=1}^{m} \omega_s \left[\frac{3}{10} \frac{\omega_s \rho_0}{R_s} + \frac{3}{2} \frac{E_s}{R_s} + \sum_{s'=1}^{\nu_s} E_{s'} M_{ss'} \right] \right] . \tag{16}$$

For the total energy per unit cell one obtains

$$E = T + \sum_{s=1}^{m} \left[-8\pi \int_0^{R_s} Z_s r \rho_s(r) dr + \int_{\omega_s} \int_{\omega_s} \frac{\rho_s(r)\rho_s(r')}{|\mathbf{r}-\mathbf{r}'|} d\tau \, d\tau' \right] + E_{xc} + C_{out} , \tag{17}$$

where C_{out} is the distant contribution to E,

$$C_{out} = \sum_{s=1}^{m} \sum_{s'=1}^{\nu_s} M_{ss'} E_s E_{s'} - \frac{6}{5} \sum_{s=1}^{m} \frac{(\omega_s \rho_0)^2}{R_s} + 3 \sum_{s=1}^{m} \frac{E_s(\rho_0 \omega_s)}{R_s} . \tag{18}$$

In the case of metals (one muffin tin per unit cell), these equations reduce to the ones given by Janak[23] and for the case of the Hartree-Fock-Slater method to those given by Asano and Yamashita.[33]

In the following we are only interested in the ordering energy. Therefore, we omit the kinetic energy and the local potential energy of the core electrons (those electrons which have no charge outside the muffin tins). Writing

$$\rho = \rho_c + \rho_b , \tag{19}$$

where ρ_c and ρ_b are the charge densities for the core and the electrons treated as band electrons, respectively, one obtains for this contribution to the total energy

$$E_b = T_b + \sum_{s=1}^{m} \left[-8\pi \int_0^{R_s} Z_s r \rho_b dr + \int_{\omega_s} \int_{\omega_s} \frac{\rho_b(r')[\rho_b(r) + 2\rho_c(r)]}{|\mathbf{r}-\mathbf{r}'|} d\tau \, d\tau' + 4\pi \int_0^{R_s} r^2 \epsilon_{xc} \rho_b \, dr \right] + E_{xc}^{out} + C_{out} , \tag{20}$$

where ϵ_{xc} is the exchange-correlation energy per electron. Using Eqs. (6) one can write

$$E_b = \sum_{i}^{\epsilon_i \leq E_F} \epsilon_i - \sum_{s=1}^{m} \left[\int_{\omega_s} \int_{\omega_s} \frac{\rho_b(r)\rho_b(r')}{|\mathbf{r}-\mathbf{r}'|} d\tau \, d\tau' + 4\pi \int_0^{R_s} (\epsilon_{xc} - \mu_{xc}) \rho_b r^2 \, dr \right] + E_{xc}^{out} + \sum_{s=1}^{m} Q_s \mu_{xc}^{out} + C_{out} - \sum_{s=1}^{m} Q_s \phi_s , \tag{21}$$

where E_F is the Fermi energy.

The difference in the ordering energy $\Delta E = E(B2) - E(B32)$ can be determined from $\Delta E = E_b(B2) - E_b(B32)$, where a self-consistent field (SCF) calculation has to be performed for the $B2$ as well as for the $B32$ phase. However using lattice constants $a_{B32} = 2a_{B2}$, ΔE can be calculated more efficiently from the differences of the first term of Eq. (21) by carrying out band-structure

calculations for $B2$ and $B32$ phases with the same muffin-tin potential.[9,10] If $N_{B2}(E)$ and $N_{B32}(E)$ are the density of states (DOS) for the $B2$ and the $B32$ phases, one obtains

$$\Delta E \approx \Delta E^{\mathrm{DOS}} = \int_{\epsilon_\Gamma(B2)}^{E_F(B2)} E N_{B2}(E) dE - \int_{\epsilon_\Gamma(B32)}^{E_F(B32)} E N_{B32}(E) dE \ , \tag{22}$$

where ϵ_Γ are the energy values at the bottom of the bands.

B. Wave functions

The wave functions ψ_i are linear combinations of the relativistic augmented plane waves $\varphi_{j,m}$,[21]

$$\psi_i = \sum_{j,m} c_{j,m} \varphi_{j,m} \ , \tag{23}$$

$$\varphi_{jm}^{(s)} = \sum_{\kappa,\mu} A_{\kappa,\mu,m}^{js} \begin{bmatrix} g_\kappa^{(s)}(r)\chi_\kappa^\mu \\ i f_\kappa^{(s)}(r)\chi_{-\kappa}^\mu \end{bmatrix} \tag{24}$$

(inside muffin tin s).

$$\varphi_{jm} = \begin{bmatrix} \chi^m \\ \boldsymbol{\sigma}\cdot\mathbf{k}_j \chi^m \end{bmatrix} \exp\{i\mathbf{k}_j\cdot\mathbf{r}\} \tag{25}$$

(outside muffin tins). The χ_κ^μ are the spin-angular functions[34] and the χ^m are the spin functions. For the SCF calculations in this paper the spin-angular part of the wave functions is simplified by using relativistic spin wave functions.[25] Within this approximation the large component of the basis function is given by

$$g_\kappa^{(s)}\chi_\kappa^\mu \approx g_l^{(s)} Y_{l,m_l} \chi^m \ . \tag{26}$$

Then the spin quantum number m of the electron states is a good quantum number and the wave function can be described by m, the wave vector $\mathbf{k}$ and the band index n:

$$\psi_i(\mathbf{r}) \approx \psi_{\mathbf{k},n,m}(\mathbf{r}), \quad m = \pm\tfrac{1}{2} \ . \tag{27}$$

For the calculation of the hyperfine properties (see below) it is helpful to use in the full relativistic procedure the wave functions, which correspond to these pure spin states. The electron states with wave-function equations (23)–(25) are twofold degenerate. For these degenerate states with wave functions ψ^{I} and ψ^{II}, we have taken those linear combinations ψ^+ and ψ^-, which diagonalized the electronic Zeeman Hamiltonian. Then the full relativistic wave functions can also be indicated by the quantum numbers $\mathbf{k}$, n, and m:

$$\psi_i(\mathbf{r}) = \psi_{\mathbf{k},n}^m(\mathbf{r}), \quad m = \pm \ . \tag{28}$$

C. Knight shift

In SI units the Zeeman energy of the nuclear moment $\boldsymbol{\mu}$ in a magnetic field $\mathbf{B}$ is given by

$$E_{\mathrm{magn}} = -\boldsymbol{\mu}\cdot\mathbf{B} \tag{29}$$

The one-electron nonrelativistic (NR) and relativistic (R) hyperfine Hamiltonians in a cubic surrounding can be written as[34]

$$\hat{H}_{\mathrm{hfs},i}^{\mathrm{NR}} = \tfrac{4}{3} F_B \frac{\boldsymbol{\mu}}{\mu_B}\cdot\mathbf{s}_i \delta(\mathbf{r}_i - \mathbf{r}_s) \ , \tag{30}$$

$$F_B = \mu_0 \mu_B^2 = 0.033\,54 \times 10^{-2}\ \mathrm{Ry}\, a_0^3 \ , \tag{31}$$

$$\hat{H}_{\mathrm{hfs},i}^{R} = ce\boldsymbol{\alpha}_i\cdot\mathbf{A}_i = \frac{m_e c}{2\pi\hbar} F_B \boldsymbol{\alpha}_i \cdot \frac{\boldsymbol{\mu}\times\mathbf{r}_i}{\mu_B r_i^3} \ , \tag{32}$$

$$\boldsymbol{\alpha}_i = \begin{bmatrix} 0 & \mathbf{s}_i \\ \mathbf{s}_i & 0 \end{bmatrix} , \tag{33}$$

where $\mathbf{s}_i$ is the spin operator and μ_B is the Bohr magneton. The Knight shift K_s can be expressed in first order as

$$K_s = \frac{\sum_i E_{\mathrm{hfs},i}}{E_{\mathrm{magn}}} \ , \tag{34}$$

where $E_{\mathrm{hfs},i}$ is the expectation value of $\hat{H}_{\mathrm{hfs},i}^{\mathrm{NR}}$ and $\hat{H}_{\mathrm{hfs},i}^{R}$, which is

$$E_{\mathrm{hfs},i} = \frac{2}{3} F_B \frac{1}{\omega} \frac{|\boldsymbol{\mu}|}{\mu_B} \langle \hat{F}_i \rangle \ . \tag{35}$$

In the nonrelativistic treatment equations (27) and (30) yield the usual Fermi contact term for $\langle \hat{F}_i \rangle$:[15]

$$\langle \hat{F}_i \rangle = \langle \hat{F}_{\mathbf{k},n,m} \rangle = 2m\omega\, |\, \psi_{\mathbf{k},n,m}(\mathbf{r}_s)\, |^2 \tag{36}$$

$\langle \hat{F}_i \rangle$ is equal to 1 for free electrons.

In the relativistic case one obtains from Eqs. (28) and (32)

$$\langle \hat{F}_i \rangle = \langle \hat{F}_{\mathbf{k},n}^m \rangle = \left\langle \psi_{\mathbf{k},n}^m \left| \frac{3m_e c\omega}{4\pi\hbar\, |\boldsymbol{\mu}|} \boldsymbol{\alpha}\cdot\frac{\boldsymbol{\mu}\times\mathbf{r}}{r^3} \right| \psi_{\mathbf{k},n}^m \right\rangle , \tag{37}$$

which is given explicitly for RAPW wave-function equations (23) and (24) elsewhere.[35]

In the next sections the bandwise contributions to the Knight shift K_s shall be considered. Therefore K_s is written as

$$K_s = \sum_n K_{s,n} \ . \tag{38}$$

For spin-restricted calculations only the single occupied states at the Fermi surface F contribute the K_s and one obtains the well-known expression[15]

$$K_{s,n} = \tfrac{2}{3} \chi_n \langle \hat{F}_n \rangle_F \tag{39}$$

$$\chi_n = F_B \frac{N_n(E_F)}{\omega} \ , \tag{40}$$

$$\langle \hat{F}_n \rangle_F = \frac{1}{F} \int_F \langle \hat{F}_{\mathbf{k}_F,n,+\frac{1}{2}} \rangle dF \ , \tag{41}$$

where χ_n and N_n are the contributions of the band n to the Pauli susceptibility and the density of states, respectively.

To include into our investigations the contribution caused by the exchange polarization of the lower valence states, self-consistent spin-polarized electron states[27–29] have been calculated by inserting a magnetic energy of

± 0.0005 Ry in the one-electron equations. Then, the self-consistent potential $V(r)$ becomes spin dependent and the susceptibility can be calculated from the difference in the number, $N_\uparrow$ and $N_\downarrow$, of spin-up and spin-down electrons in the band n:

$$\chi'_n = F_B \frac{N_\uparrow - N_\downarrow}{\omega \mu_B B} . \tag{42}$$

The difference between χ'_n [Eq. (42)] and χ_n [Eq. (40)] is caused by the exchange enhancement effect.[36,37]

Within this method the Knight shift can be calculated as an integral over all occupied states in $\mathbf{k}$ space (an integral over the Fermi volume):

$$K_{s,n} = \frac{2}{3} \frac{F_B}{\mu_B B \omega \omega^*} \left[\int_{\omega^*_{n\uparrow}} \langle \hat{F}_{\mathbf{k},n,+} \rangle d\tau^* + \int_{\omega^*_{n\downarrow}} \langle \hat{F}_{\mathbf{k},n,-} \rangle d\tau^* \right] , \tag{43}$$

where ω^* is the volume of the Brillouin zone and $\omega^*_{n\uparrow}$ and $\omega^*_{n\downarrow}$ are the Fermi volumes of the nth band for the spin-up and spin-down electrons. In the nonrelativistic theory the expression inside the large parentheses is equal to the spin density at the nucleus considered multiplied by ω. According to Eqs. (39)—(43), three different values for the Knight shift have been calculated: (I) the direct contribution, Eq. (39); (II) the direct contribution using the exchange enhanced susceptibility, Eq. (42); and (III) the value deduced from the spin-polarized procedure, Eq. (43).

Comparing method I with methods II and III one obtains the influence of the exchange enhancement of the susceptibility on the value of K_s. Method II takes only the enhancement of the susceptibility into account, whereas method III gives in addition the exchange polarization of the inner valence states.

Besides the different procedures to sum over the electron states to get K_s, we also investigated the influence of the use of the different types of wave functions ψ_i [Eqs. (27) and (28)] on the calculated hyperfine fields. This means that the expectation value $\langle \hat{F}_i \rangle$ can either be calculated from the SRAPW wave functions using Eq. (36) or from the RAPW wave functions using Eq. (37).

D. Numerical details

In this section the input data for the RAPW calculation are listed. For the SCF calculation the following electrons are treated as band electrons:

Tl: $5d^{10}6s^2 6p^1$,

Na: $3s^1$,

Li: $2s^1$.

The lattice constants are $a(\mathrm{LiTl}) = 6.472 a_0$ and $a(\mathrm{NaTl}) = 14.15 a_0$. The muffin-tin radii are always taken as half the nearest-neighbor distance.

The fcc unit cell for the NaTl-type structure is one-fourth of the unit cell given in Fig. 1 with two formula units NaTl. For a $B2$ phase as LiTl the simple cubic unit cell with one formula unit LiTl is used. However, to ensure that the accuracy as well as the convergence are the same for the $B2$ and $B32$ calculations, we have done test calculations for LiTl for the larger fcc unit cell with the atomic arrangement corresponding to the $B2$ structure (see Fig. 1). Therefore, the following data correspond to the calculations in the fcc unit cell. The $\mathbf{k}$ points, for which the SCF calculation have been performed, have been chosen equidistant in $\mathbf{k}$ space. Most calculations have been done for 89 $\mathbf{k}$ points in the irreducible $\frac{1}{48}$th of the Brillouin zone. Integration over $\mathbf{k}$ space has been performed by extending the tetrahedron method of Lehmann and Taut[38] to volume integrals.

The majority of calculations have been done with a maximum angular momentum $l_{\max} = 5$. The number of RAPW basis functions is chosen according to the Switendick criterion[39] $S = 5$ (about 60 reciprocal-lattice vectors $\mathbf{k}$).

The convergence and accuracy of the calculations have been checked by bisecting the mesh width in $\mathbf{k}$ space, by increasing $l_{\max}$ to 10, and by setting $S = 6$. A change in the difference of the ordering energy and in the Knight shift of less than 5% is found.

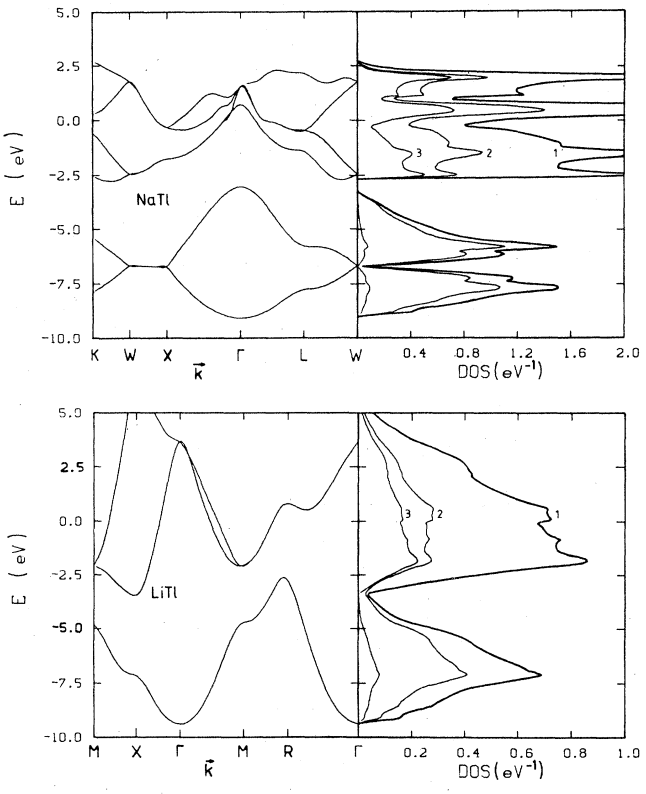

FIG. 2. Left: Band structure of the first three valence bands of LiTl and the first six valence bands for NaTl. The zero of the energy scale is the Fermi energy E_F. Right: Density of states (DOS) $N(E)$ for the bands shown on the left-hand side. Curve 1, total DOS per unit cell; curve 2, partial DOS for the Tl sphere; curve 3, partial DOS for the alkali sphere.

III. RESULTS

The band-structure calculations for LiTl and NaTl have been performed by the self-consistent scalar relativistic augmented-plane-wave method (SRAPW). The resulting band structure and the density of states (DOS) for the valence electrons are shown in Fig. 2. These bands do not overlap with the $5d$ bands of Tl, which are not shown here. Since the size of the unit cells for LiTl and NaTl are different, one band of LiTl corresponds to two bands for NaTl. Comparing NaTl and LiTl one can see that the different bands overlap more in LiTl than in NaTl. For NaTl the bands show only a small overlap and the Fermi energy lie between the 4th and 5th band in a region of low DOS, which is also found for the Zintl-phase LiAl.[40]

Figure 3 shows a comparison between the DOS(SRAPW) and the DOS(RAPW). Differences between the SRAPW and RAPW approaches are found for the higher valence bands and the DOS at the Fermi surface. For NaTl the DOS at the Fermi energy is smaller by a factor of 2 for the RAPW calculation. The differences between the SRAPW and the RAPW results are caused by the spin-orbit coupling. It is also found for PbTe (Ref. 41) that the omission of the spin-orbit coupling mostly influences the higher valence bands.

In addition to the total DOS, the local DOS[42]

$$q_s(E)=N(E)\int_{\omega_s}\rho(\mathbf{r},E)d\tau \tag{44}$$

is shown in Fig. 2. $\rho(\mathbf{r},E)$ is the electron density of the states with energy eigenvalue E, $N(E)$ is the DOS, and ω_s is the volume of the muffin-tin sphere s. From the curves q_s as a function of E one can see that the charge distribution is significantly different for the lower valence bands (1st band of LiTl and 1st and 2nd bands of NaTl) and the upper valence bands (2nd and 3rd bands of LiTl and 3rd and 4th bands for NaTl). For the lower bands $q_{\mathrm{Tl}}(E)$ is much larger than $q_{\mathrm{alkali}}(E)$, that is, the charge for these states is more or less concentrated on the thallium spheres. This effect is more pronounced in NaTl than in LiTl. On the other hand, for the upper valence bands the electronic charge is much more evenly distributed between the thallium and alkali spheres.

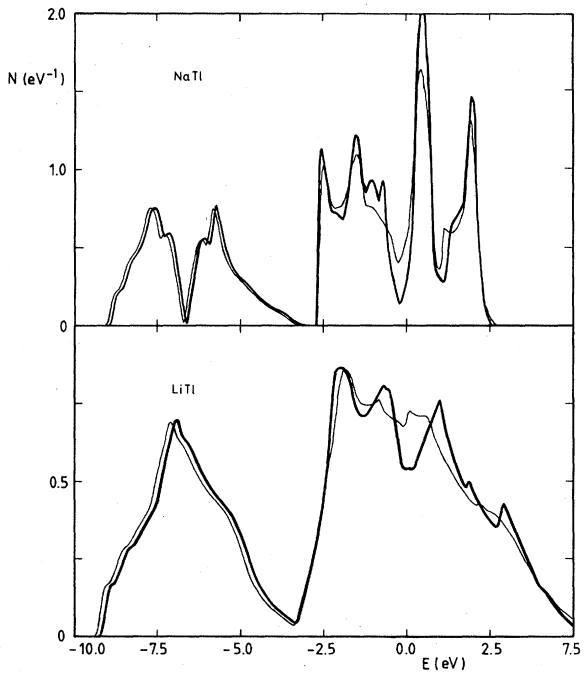

FIG. 3. Density of states $N(E)$ per formula unit AB for the first three valence bands of LiTl and for the first six valence bands of NaTl. Thick line $N(E)$ deduced from the full RAPW procedure; thin line, $N(E)$ deduced from the scalar RAPW (SRAPW) procedure.

The resulting character of the chemical bond can be seen in Fig. 4, where contour maps of the charge density ρ are plotted for the (101) plane for some electron states for the lower and upper valence bands. For a pure metallic bond the charge distribution should be nearly constant outside the regions of the ionic cores. The sizes of the ionic cores are plotted in Fig. 4(a). The charge-density contour lines shown in Fig. 4 are normalized to a constant charge density $\rho_0=1/\omega_{B2}$.

For NaTl one finds for the electron states of the lower valence bands strong covalent bonds of nearly pure s character formed by the diamondlike Tl sublattice. For the states of the upper bands the bonds are more metalliclike. This metallic character is indicated in Fig. 4 by the fact that the characteristic bonding directions are less pronounced for these states especially in the region outside the ionic cores. In the region between like atoms the

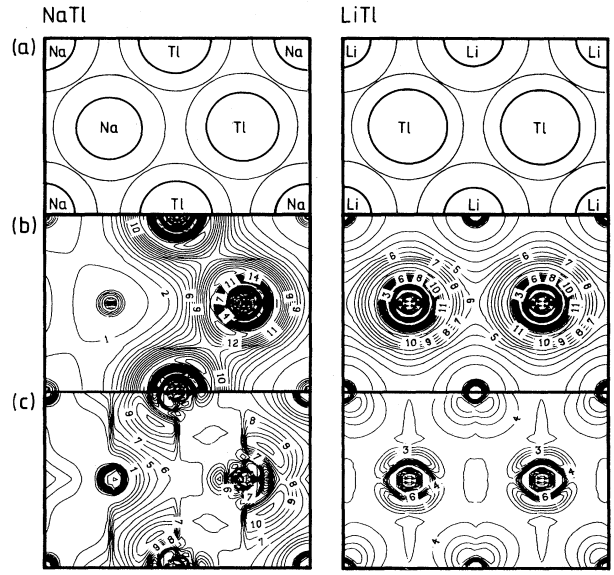

FIG. 4. Display of contour lines of the charge density ρ for one electron for the (101) plane for LiTl and NaTl calculated by the SRAPW procedure. The numbers at the contour lines correspond to the normalization $\rho'=5\rho/\rho_0$, where ρ_0 is equal to the constant distribution of the charge of one electron in LiTl and NaTl; $\rho_0=1/a^3$ for LiTl and $\rho_0=1(a/2)^3$ for NaTl with values of a given in Table II. It follows that the contour line with $\rho=\rho_0$ is labeled by the number 5. (a) Atomic positions in the (101) plane thin-line circles, muffin-tin spheres; thick-line circles, sizes of the atomic cores Li^+, Na^+, and Tl^{3+}. (b) Contour lines for ρ' for an electron state of the first valence band. (c) Contour lines for ρ' for an electron state near the Fermi surface.

charge density shows only small fluctuations. However between the Na atoms ρ is distinctly smaller than ρ_0, whereas $\rho > \rho_0$ between the Tl atoms. Furthermore, one finds a gradient in the charge density in the region from the Tl to the Na atoms.

For LiTl the bonds are more metalliclike than for NaTl in the sense that in LiTl the electronic charge outside the ionic cores is more uniformly distributed than in NaTl. Even for the lower valence band one finds for LiTl a distinct amount of charge in the Li atomic sphere.

The charge distribution is given quantitatively in Table II. The total amount of charge inside the Na sphere in NaTl is equal to 0.5 (column 7 in the last line of Table II), which is less than the charge inside the Li sphere in LiTl (=0.7), although the muffin-tin sphere of Li is smaller than that of Na. Besides this band-structure result listed in Table II, we have also calculated the charge distribution for LiTl and NaTl, which one obtains from overlapping the charge densities of the free atoms. Then one calculates the charge inside the atomic spheres without any charge transfer. This yields $q(\mathrm{Na})=0.6$ for Na in NaTl and $q(\mathrm{Li})=0.7$ for Li in LiTl, and shows that a charge transfer takes place in NaTl from the Na atoms to the Tl atoms but no distinct charge transfer could be found in LiTl. However, the charge transfer in NaTl is less than for an ionic phase Na^+Tl^-; see also Ref. 43. The charge-transfer effect for NaTl can be seen in Fig. 5, where the charge density of the valence electrons is plotted for the direction of nearest neighbors [111]; see Fig. 1. One can very clearly see the small amount of charge in the nonbonding region between the Na atoms.

In Tables III–VI the results for the calculated hyperfine fields are presented. Table III contains the hyperfine expectation values for one **k** point for LiTl. From this table the different contributions to the hyperfine fields as well as the differences in the fields gained from the SRAPW and RAPW procedures can be studied. Although the SRAPW and the RAPW procedures give similar results for the charge distributions and the density of states, the calculated hyperfine fields are quite different for both methods; the reasons are discussed below.

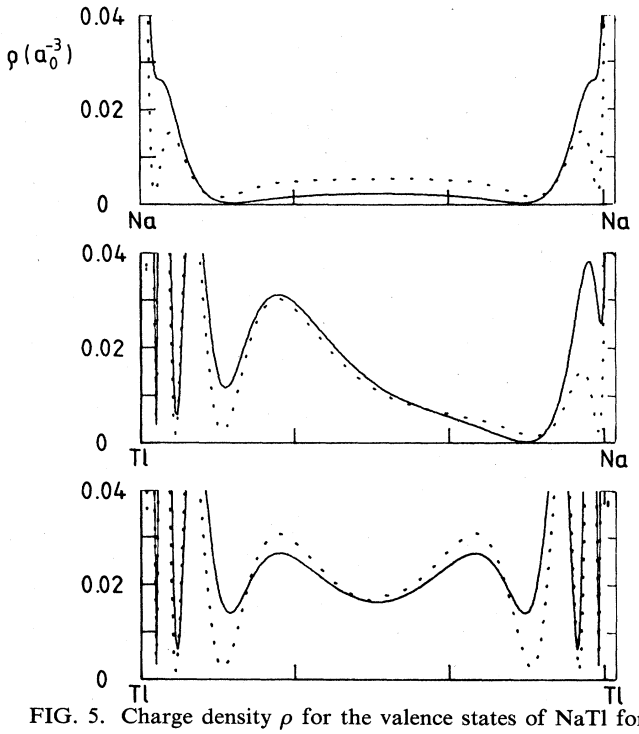

FIG. 5. Charge density ρ for the valence states of NaTl for the (111) direction calculated by the SRAPW procedure. ρ is plotted from one nucleus site to the next nucleus site. The solid lines show the band-structure results whereas the dotted lines give the result from overlapping the charge densities of the free atoms Na and Tl.

It is found that for most electronic states the s contribution to the hyperfine field is large compared to others. This is also found for PbTe.[44] However, for those electronic states having a small amount of s-like charge, the p contributions to the hyperfine fields are of the same size.

TABLE II. Charge inside and outside the atomic spheres Q_s and Q_{out} for the SRAPW and the RAPW calculations for LiTl and NaTl for lattice constants $a(\mathrm{LiTl})=6.472a_0$ and $a(\mathrm{NaTl})=14.15a_0$ and volumes of the atomic spheres $\omega_{\mathrm{Li}}(\mathrm{LiTl})=\omega_{\mathrm{Tl}}(\mathrm{LiTl})=84.134a^3$ and $\omega_{\mathrm{Na}}(\mathrm{NaTl})=\omega_{\mathrm{Tl}}(\mathrm{NaTl})=113.569a^3$. All values are given per formula unit LiTl and NaTl.

	SRAPW				RAPW			
LiTl	Number of electrons	Q_{alkali}	Q_{Tl}	Q_{out}	Number of electrons	Q_{alkali}	Q_{Tl}	Q_{out}
				(a) LiTl				
1st band	2.000	0.211	1.228	0.561	2.000	0.210	1.230	0.560
2nd band	1.675	0.430	0.550	0.695	1.739	0.413	0.630	0.696
3rd band	0.325	0.072	0.129	0.124	0.261	0.061	0.098	0.102
Total	4.000	0.713	1.907	1.380	4.000	0.684	1.958	1.358
				(b) NaTl				
1st band	1.000	0.061	0.707	0.232	1.000	0.061	0.707	0.232
2nd band	1.000	0.046	0.761	0.193	1.000	0.046	0.761	0.193
3rd band	0.994	0.224	0.399	0.371	1.000	0.206	0.432	0.362
4th band	0.954	0.141	0.443	0.370	0.980	0.143	0.473	0.364
5th band	0.052	0.014	0.020	0.018	0.020	0.007	0.006	0.007
6th band	0.0004	0.000	0.000	0.000	0.000	0.000	0.000	0.000
Total	4.000	0.486	2.330	1.184	4.000	0.463	2.379	1.158

TABLE III. Charge distribution and hyperfine expectation values for LiTl for one $\mathbf{k}$ point, $\mathbf{k}_n=(\frac{1}{4},\frac{1}{4},\frac{1}{8})(2\pi/a)$, for the first and second band, $n=1,2$. The values for the scalar relativistic (SRAPW) and the full relativistic (RAPW) procedure are listed.

(a) Charges

	Energy	Charge inside atomic sphere of Li				Charge inside atomic sphere of Tl			
		s-like	p-like			s-like	p-like		
Method	$\epsilon_{n,\mathbf{k}}$	s	$p_{1/2}$	$p_{3/2}$		s	$p_{1/2}$	$p_{3/2}$	
SRAPW	−0.080 22	0.071		0.054		0.513		0.031	
	0.502 81	0.000		0.242		0.000		0.286	
RAPW	−0.080 21	0.070	0.037		0.017	0.510	0.019		0.014
	0.484 53	0.015	0.118		0.081	0.019	0.093		0.225

(b) Contributions $(\kappa-\kappa')$ to the hyperfine expectations values, Eqs. (36) and (37)

	Energy	Li nucleus				Tl nucleus				
Method	$\epsilon_{n,\mathbf{k}}$	$(s_{1/2}-s_{1/2})$	$(p_{1/2}-p_{1/2})$	$(p_{3/2}-p_{3/2})$	$(p_{3/2}-p_{1/2})$	Total	$(s_{1/2}-s_{1/2})$	$(p_{1/2}-p_{1/2})$	$(p_{3/2}-p_{3/2})$	$(p_{3/2}-p_{1/2})$	Total
SRAPW	−0.080 22	12.5				12.5	69 730				69 730
	0.502 81	0.0				0.0	0				0
RAPW	−0.080 21	11.7	0.1	−0.2	−0.1	11.4	10 140	19	−36	−5	10 110
	0.484 53	3.3	0.8	−2.1	−0.3	1.6	545	74	−1361	−61	−804

A large cancellation between the different p contributions by integrating over $\mathbf{k}$ space is found. Such a large p contribution is missing in PbTe, because the electronic states at the Fermi surface (L6+ in Fig. 1 of Ref. 41) have a dominant s component.

The data which one obtains from the Fermi-contact Hamiltonian using SRAPW wave functions are much larger than the ones resulting from using the correct relativistic method. The large difference in the values of $\langle\hat{F}_i\rangle$ for Tl is caused by the following three effects: (a) the density at the Tl nucleus is about 3 times larger for the SRAPW wave functions than for the RAPW wave functions; (b) the omission of the dipolar terms[35] by using the Hamiltonian in Eq. (30) instead of Eq. (32); (c) the slight divergence of the relativistic wave functions near the nucleus.

The results for the hyperfine fields from RAPW wave functions are also compared with those from relativistic orthogonalized-plane-wave wave functions (ROPW). Since calculated hyperfine fields from ROPW's are available for Cs metal,[45] we have calculated the hyperfine fields $\langle\hat{F}_i\rangle$, Eq. (37), for this metal. Tterlikkis *et al.*[45] have gotten for the value of $F'=8\pi\langle\hat{F}_i\rangle/3$ from ROPW $F'(\mathrm{Cs})=18\,571$, whereas our results from non-self-consistent RAPW calculation give $13\,500<F'<19\,500$, depending on the direct in $\mathbf{k}$ space.

In Tables IV–VI the results for the Knight shift calculated by methods I–III (see Sec. II) are given. For comparison purposes, the experimental results are also listed. From the results for both alloys (LiTl and NaTl), one can deduce the following general trends. The values gained from the scalar relativistic wave functions (SRAPW) are much larger than the experimental results. This was expected, as was shown above by the analysis of the hyperfine fields. Furthermore, the values for K_s(Tl) gained from the integration over the Fermi volume (method III) are closer to the K_s(expt.) than those gained from the integration over the Fermi surface (methods I and II). The reasons for this are twofold: Firstly, there is a large exchange polarization contribution of about −0.23% per electron of the lower valence bands (Tl 6s bands). Secondly, for those bands for which a small s character is found at the Fermi energy or for which the DOS(E_F) is small, the contribution from polarization effects from these bands can be of the same order as the direct contribution from the Fermi surface.

Comparing the theoretical and the experimental results, one finds good agreement only for LiTl. For NaTl we have given two different values for the total theoretical result. The first value K_s(Tl)=0.99% belongs to the stoichiometric phase NaTl with 4 valence electrons per half fcc unit cell ($N_{VE}=4$), i.e., 1 "molecule" per half unit cell. The largest contribution in this case comes from the 5th band, which is only occupied by 0.02 electrons per half unit cell (see Table II). However it is known, that the IA-IIIA compounds of the NaTl type are "defect phases".[46,47] In these phases vacancies at the positions of the alkali-metal atoms of 2–4 % are present.[46,47] As discussed by Asada *et al.*[40] for the case of LiAl, the Fermi energy is shifted according to the smaller N_{VE}. Assuming 4% vacancies for NaTl at the Na sites ($N_{VE}=3.96$), the

TABLE IV. Paramagnetic spin-susceptibility χ and Knight shift K_s for LiTl calculated by three different methods (see Sec. II). Method I, integration over Fermi surface [Eqs (39) and (40)]; method II, including the exchange enhancement of χ [Eqs. (39) and (42)]; method III, integration over Fermi volume [Eq. (43)]. The values are given for the scalar relativistic (SRAPW) and full relativistic (RAPW) procedure.

	$10^6\chi$		10^2K_s					
	χ_n	χ'_n	Method I		Method II		Method III	
	Eq. (40)	Eq. (42)	^{7}Li	^{205}Ti	^{7}Li	^{205}Tl	^{7}Li	^{205}Tl
SRAPW								
1st band							0.0003	−3.00
2nd band	2.87	7.20	0.0018	0.65	0.0046	1.62	0.0041	1.44
3rd band	3.08	7.40	0.0026	4.60	0.00061	11.06	0.0059	10.61
Total			0.0044	5.25	0.0107	12.68	0.0103	9.05
RAPW								
1st band							0.0010	−0.46
2nd band	2.04	5.05	0.0016	0.05	0.0039	0.12	0.0036	0.32
3rd band	2.52	6.19	0.0015	0.51	0.0037	1.24	0.0037	1.17
Total			0.0031	0.56	0.0076	1.36	0.0083	1.03
K_s (Expt.)[a]			$\ll$0.025	1.2	$\ll$0.025	1.2	$\ll$0.025	1.2

[a]References 2 and 5; $K_s(^7\text{Li})$ is found to be very small compared to $K_s(^7\text{Li})$ in Li metal.

TABLE V. Bandwise contributions to the paramagnetic susceptibility χ_n and Knight shift $K_{s,n}$ for NaTl. The SRAPW and RAPW results are listed in the first and second line, respectively. χ_n and $K_{s,n}$ are calculated by three different methods; see caption of Table IV.

			$10^2K_{s,n}$					
			Method I		Method II		Method III	
Band n	$10^6\chi_n$	$10^6\chi'_n$	^{23}Na	^{205}Tl	^{23}Na	^{205}Tl	^{23}Na	^{205}Tl
1							0.0006	−1.66
							0.0005	−0.25
2							0.0006	−1.98
							0.0004	−0.27
3	0.33	0.47	0.001	0.332	0.0026	0.46	0.0008	0.60
							0.0001	0.04
4	1.76	2.18	0.0003	2.048	0.0004	2.536	0.0002	2.56
	0.78	0.85	0.0009	0.168	0.0010	0.183	0.0011	0.20
5	4.91	5.59	0.1172	12.58	0.1332	14.330	0.1242	13.82
	2.90	3.31	0.0882	1.14	0.1007	1.30	0.0993	1.26
6	0.06	0.09	0.0022	0.16	0.0032	0.254	0.0002	0.18
	0.001	0.001	0.003	0.00	0.0003	0.00	0.0006	0.01
Sum	7.006	8.33	0.12	15.12	0.14	17.58	0.13	13.52
	3.69	4.17	0.09	1.31	0.10	1.48	0.10	0.99

TABLE VI. Knight shift K_s for NaTl from full relativistic APW calculations (method III in Sec. II) for different numbers of valence electrons per half fcc unit cell (N_{VE}).

N_{VE}	10^2K_s(Na)	10^2K_s(Tl)
4	0.10[a]	0.99[a]
3.96	0.0025[b]	−0.14[b]
Expt.[c]	−0.016	−0.96

[a]Last line from Table V.

[b]The bandwise contributions are $K_{s,1}$, $K_{s,2}$, and $K_{s,3}$ as given in Table V; $K_{s,5}=0$ and $K_{s,4}(^{23}\text{Na})=0.0017\%$ and $K_{s,4}(^{205}\text{Tl})=0.34\%$.

[c]References 2 and 5.

Fermi energy is shifted below the 5th band, and a total $K_s(\text{Tl,theor.})=-0.14\%$ results. This means that the negative contribution from the exchange polarization becomes larger than the Fermi contact term.

Finally in Tables VII and VIII the differences in the ordering energies ΔE for LiTl and NaTl are shown. In Table VII the results of ΔE on the basis of Eq. (22) are given, and in Table VIII the different energy terms from Eqs. (20) and (21) are listed.

We have performed the SCF calculations for both structures, $B2$ and $B32$. However, for the data given in Table VII, one needs only one muffin-tin potential (see Sec. II). Therefore, we have listed in Table VII the calcu-

TABLE VII. Differences in the ordering energy $\Delta E^{\mathrm{DOS}}=E(B2)-E(B32)$ in eV per formula unit for LiTl and NaTl on the basis of different self-consistent muffin-tin potentials using the scalar relativistic (SRAPW) as well as the full relativistic (RAPW) procedure.

Line	Compound	Potential	Method	$B(E2)-E(B32)$
1	LiTl	LiTl($B2$)	SRAPW	−0.278
2			RAPW	−0.300
3		LiTl($B32$)	SRAPW	−0.181
4	LiTl ($a=7.075a_0$)	LiTl($B2$)	SRAPW	−0.159
5	NaTl	NaTl($B32$)	SRAPW	0.058
6			RAPW	0.010[a]
				−0.001[b]
7		NaTl($B2$)	SRAPW	0.022

[a]"Defect phase" NaTl.
[b]Stoichiometric NaTl.

TABLE VIII. Total energy E_b, the kinetic energy T_b of the electrons treated as band electrons ($5d$ electrons of Tl and valence electrons), and the distant energy term C_{out} [see Eqs. (17) and (18)] for LiTl and NaTl for the $B2$ and the $B32$ structures.

	LiTl($B2$)		LiTl($B32$)	NaTl($B2$)		NaTl($B32$)
Lattice constant a/a_0	6.472		12.944	7.075		14.15
Kinetic energy T_b/Ry	228.30		228.89	228.14		228.05
$T_b(B2)-T_b(B32)$		−0.59			+ 0.09	
Total energy E_b/Ry	−99.266		−99.232	−99.282		−99.293
$E_b(B2)-E_b(B32)$		−0.032			+ 0.011	
Distant term C_{out}/Ry	−0.812		−0.668	−0.359		−0.319
$C_{\mathrm{out}}(B2)-C_{\mathrm{out}}(B32)$		−0.144			−0.040	

lated values ΔE as a function of the used muffin-tin potential. The influence of the different procedures, SRAPW or RAPW, can also be seen from Table VII. All data in Table VII show the same trend, that is ΔE is negative for LiTl and positive for NaTl. However, for the RAPW calculation for NaTl one obtains the "correct" sign for ΔE only for the "defect-phase" NaTl.

The shape of ΔE as a function of the N_{VE} can be studied in Fig. 6. Here ΔE is plotted as a function of the upper limit (Fermi energy) of the integral; see Eq. (22). Since the Fermi energy is a function of N_{VE}, $N_{VE}=\int_{\epsilon_\mu}^{E_F} N(E)dE$. ΔE is displayed directly as a function of N_{VE}.

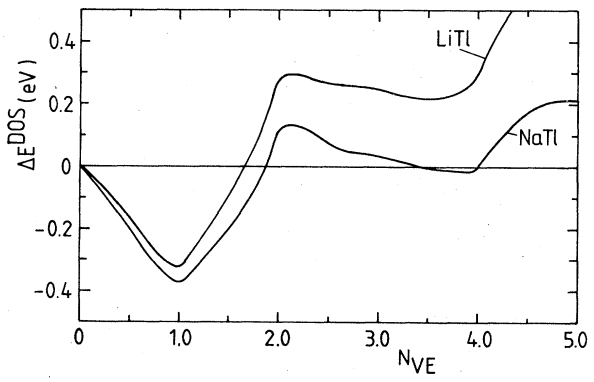

FIG. 6. Differences in the energy ΔE^{DOS}, Eq. (22), between the $B2$ and $B32$ structure as a function of the number of occupied states [number of valence electrons per unit cell $\omega_{B2}(N_{VE})$], where the DOS are calculated using the muffin-tin SCF potentials of LiTl and NaTl, respectively. For stoichiometric LiTl and NaTl the N_{VE} is equal to 4.

IV. DISCUSSION

A. Chemical bond

As pointed out in the Introduction, the chemical bond in LiTl should be dominantly metalliclike, whereas in NaTl covalent contributions to the chemical bonds and a charge transfer from the Na to the Tl atoms are expected to be important. The results given in the preceding section confirm these general observations. However, it was found theoretically that the charge transfer from the Na to the Tl atoms is much less than the charge of one electron and no saturated sp hybrid could be found for the Tl sublattice. The calculations show that in NaTl the $6s$ electrons of Tl form covalent valence bands, which are separated by a band gap from the upper valence bands. The wave functions of the states of the lower $6s$ bands are predominantly s-like functions. The valence states of the upper bands are sp-hybrid bands of Tl and Na, and the character of the chemical bond of these states is similar to those of the $B2$-phase LiTl.

It is interesting to note that a covalent Tl—Tl bond and a charge transfer from the alkali atoms to the Tl atoms were also found for a hypothetic phase LiTl($B32$). How-

ever, these effects are not so pronounced as in NaTl.

In analyzing the stability of Zintl-phases AB, it is argued that the nearest neighbors should be in contact,[8] and therefore the size of the atoms A and B should be the same. In Table IX covalent bond radii r_{cov}, ionic radii r_{ion}, and metallic bond radii r_{met} are listed together with the half distance length r_{B32} of the atoms in NaTl and LiTl($B32$). These values r_{B32} should be the radii of the atoms in the corresponding compounds. For NaTl, r_{B32}(Tl) is smaller than r_{met}(Tl) and larger than r_{cov}(Tl), as is expected for a mixture of covalent and metallic bonds. Also r_{B32}(Na) is smaller than r_{met}(Na) because the Na atoms in NaTl carry less charge than in Na metal. On the other hand, for LiTl($B32$), r_{B32}(Tl) is nearly equal to r_{cov}(Tl) and a distinct compression of the Tl atoms in LiTl($B32$) should result. This point is discussed in more detail below.

B. Knight shift

For LiTl the theoretical and the experimental results for K_s(Li) and K_s(Tl) agree quite well. Therefore, we conclude that the orbital and diamagnetic contributions to the Knight shift are not important for this compound. Discussing the results for LiTl in more detail, one can see that K_s(Tl,theor.) calculated from the simple integration over the Fermi surface is larger than K_s(Tl,expt.) because the large negative exchange polarization of the lower valence bands is missing if one integrates only over the Fermi surface. In addition to this exchange polarization effect, the value for K_s in LiTl shows the normal behavior of metals and alloys with dominant sp character for the valence electrons. The value K_s(Li) is very small, because the partial s density for the Li sphere is small for the states at the Fermi surface.

For NaTl the situation is different. The theoretical results for the stoichiometric phase NaTl for K_s(Tl) and K_s(Na) are similar to the results in the corresponding metals, which, however, are not found experimentally in NaTl. The mechanism which leads to this large positive calculated hyperfine field is the contribution of the 5th valence band, which has a large s character.

For the defect-phase NaTl one obtains for K_s(Na) in NaTl the correct order of magnitude, that is, the Knight shift is nearly 0. This result is caused by the extremely small density of states at the Fermi surface and because of the small partial s charge (not total charge) for these states. For K_s(Tl) in NaTl the theoretical result has the same sign as the experimental one. However, the absolute value of K_s(Tl, theor.) is much smaller than K_s(Tl,expt.). Therefore we conclude that the large negative value K_s(Tl, expt.) in NaTl is caused by the extremely small density of states at the Fermi surface, the large exchange polarization contribution of the lower valence bands (the $6s$ bands of Tl) and by a diamagnetic contribution, which has the same order of magnitude as the exchange polarization effect. The diamagnetic contribution is large, because in the defect-phase NaTl the 4th valence band is nearly filled and a small effective mass is expected for the states at the Fermi surface.

TABLE IV. Atomic radii for Li, Na, and Tl (Refs. 48 and 49) and half bond length Li—Li, Na—Na, and Tl—Tl in NaTl($B32$) and LiTl($B32$) (in Å).

	Li	Na	Tl
Metallic bond radius for 8-coordination r_{met}	1.52	1.86	1.66
Covalent tetrahedral bond radius r_{cov}			1.47
Ionic radius Me^+ r_{ion}	0.78	0.96	
Half bond distances r_{B32}			
Me—Me in LiTl($B32$)	1.49		1.49
in NaTl ($B32$)		1.62	1.62

C. Ordering energy

The differences in the ordering energy ΔE listed in Table VII are smaller in magnitude than those deduced from pseudopotential theory,[8] and the values of ΔE(NaTl) are within the order of magnitude, which one expects for differences in the ordering energy for real phase transitions. However, the values which one obtains from the SCF energies (Table VIII) are much larger. The reasons for this result are as follows: (a) The procedure to calculate ΔE for fixed lattice constants $a_{(B32)}=2a_{(B2)}$ instead of using the lattice constants of the minimum in energy should influence the result in ΔE given in Tables VII and VIII differently; (b) the muffin-tin approximation affects the one-electron energies ϵ_i and the integral equation (22) and the total energy according to Eq. (21) differently; (c) the influence of the $5d$ electrons of Tl is only included in the values given in Table VIII; (c) ΔE has always been calculated by a difference of two large numbers. These large numbers are by a factor of 100 larger for the values given in Table VIII than those of Table VII.

Nevertheless all data from Tables VII and VIII show the same trends. The most reliable theoretical values for ΔE should be those in Table VII deduced from the full RAPW procedure.

Next we shall consider two different aspects of the problem of the size of ΔE, namely, the role of the size of the atoms and the role of the details of the electron bands.

It can be seen from Table VII that the absolute value of ΔE is significantly larger for LiTl than for NaTl. Looking at the kinetic energy (Table VII) one finds that for LiTl, $T_b(B32)$ is much larger than $T_b(B2)$. This larger value of T for the $B32$ phase is accompanied by a gain in potential energy V according to the virial theorem[22,23]

$$\tfrac{3}{2}p\omega = T + \tfrac{1}{2}V' , \tag{45}$$

$$V' = V - 6\int \rho(\epsilon_{xc}-\mu_{xc})d\tau . \tag{46}$$

However, as discussed above, the Tl atoms are compressed in LiTl($B32$). Then [in addition to the second term in Eq. (46)] the gain in $\Delta V = V_b(B32) - V_b(B2)$ is less than $-2\Delta T_b$, because the internal pressure p is larger for the $B32$ phases than for the $B2$ phase. Therefore, the large positive values of ΔE for LiTl follows as a consequence of the fact that the Tl atoms are larger than the Li atoms.

It would be interesting to calculate ΔE as a function of

the lattice constant a. Since the $5d$ electrons of Tl have to be included in such SCF calculations, these calculations become very time consuming within the RAPW procedure and could not be performed in this work. However, using the muffin-tin potential of LiTl ($a=6.472$), we have calculated the band structure and ΔE for LiTl for the larger lattice constant $2a_{B2}=a_{B32}=14.15a_0=a$(NaTl). The results are given in Table VII (line 4). As expected, ΔE is smaller for the larger lattice constant (compare lines 1 and 4 of Table VII).

The situation is different in NaTl. Taking the size of the atoms into consideration we can draw the following conclusions: (a) in pure metallic bonds the more electropositive element Na is larger than Tl. Because a charge transfer takes place in Zintl phases (see above), the sizes of the partly ionic Na atoms in NaTl are expected to be smaller than in Na metal; (b) the Tl atoms are not compressed in the $B32$ phase, because the Tl-Tl nearest distance is just as large as one expects for a mixture of covalent and metallic electron bonds; see above. As a consequence the differences in the kinetic energy terms for NaTl are much smaller than for LiTl; see Table VIII. Therefore, in NaTl the size effect is not important in discussing the favored structure $B2$ or $B32$.

It is very difficult to find one single physical mechanisms, which gives an explanation for the difference in the electronic energy between the $B2$ and the $B32$ phase for NaTl. The differences in the various energy terms given in Eqs. (20) and (21) are much larger than ΔE, and ΔE is not caused by one single term. As an example the distant terms C_{out} are listed in Table VII. One finds $C_{\text{out}}(B2)-C_{\text{out}}(B32)=-0.04$ Ry, whereas ΔE is only 0.01 Ry. It can be seen that the term C_{out}, which includes the Madelung energy, favors the $B2$ structure in accordance with the general observation that the ionic contribution to the lattice energy favors an arrangement of the atoms, for which the nearest neighbors are of unlike type.

Comparing the band structure and density of states of NaTl and NaTl($B2$), one finds that the bands for the $B32$ structure are narrower and steeper than the bands for the $B2$ structure, and that the bands of the $B32$ structure show a smaller overlap than those for the $B2$ structure. It follows that the energy difference ΔE as a function of the Fermi energy or as a function of the number of occupied states is an oscillating function for NaTl (see Fig. 6) and $\Delta E<0$ for stoichiometric NaTl.

ACKNOWLEDGMENTS

The author wishes to thank Professor Dr. Helmut Witte for many helpful discussions and Professor Dr. Alarich Weiss for continuous support and interest in the present work.

[1]E. Zintl and P. Woltersdorf, Z. Elektrochem. **41**, 876 (1935).
[2]L. H. Bennett, Acta Metall. **14**, 997 (1966).
[3]R. E. Watson, L. H. Bennett, G. C. Carter, and I. D. Weisman, Phys. Rev. B **3**, 222 (1971).
[4]N. Bloembergen and T. J. Rowland, Phys. Rev. **97**, 1679 (1955).
[5]L. H. Bennett, Bull. Am. Phys. Soc. **11**, 172 (1966).
[6]P. W. Anderson, *Concepts in Solids* (Benjamin, New York 1963), p. 6; L. Brewer, in *High Strength Materials,* edited by V. Zackay (Wiley, New York, 1964), p. 37; N. Engel, in *Developments in the Structural Chemistry of Alloy Phases,* edited by B. Giessen (Plenum, New York, 1969), p. 25—40; W. Hückel, *Structural Chemistry of Inorganic Compounds,* (Elsevier, Amsterdam, 1951), pp. 829ff.
[7]A. B. Makhnovetskii and G. K. Krasko, Phys. Status Solidi B **80**, 341 (1977).
[8]M. B. McNeil, W. B. Pearson, L. H. Bennett, and R. E. Watson, J. Phys. C **6**, 1 (1973).
[9]V. Heine, in *Solid State Physics,* edited by H. Ehrenreich, F. Seitz, and D. Turnbull (Academic, New York, 1980), Vol. 35, p. 1.
[10]D. G. Pettifor, J. Phys. C **3**, 367 (1970).
[11]P. Hohenberg and W. Kohn, Phys. Rev. **136**, B864 (1964).
[12]W. Kohn and L. J. Sham, Phys. Rev. **140**, A1133 (1965).
[13]N. Bloembergen and T. J. Rowland, Acta Metall. **1**, 731 (1953).
[14]A. M. Clogston and V. Jaccarino, Phys. Rev. **121**, 1357 (1961).
[15]W. D. Knight, in *Solid State Physics,* edited by F. Seitz and D. Turnbull (Academic, New York, 1956), Vol. 2, p. 93.
[16]S. D. Mahanti and T. P. Das, Phys. Rev. B **3**, 1599 (1971).
[17]T. P. Das and E. H. Sondheimer, Philos. Mag. **5**, 529 (1960).
[18]Y. Yafet and V. Jaccarino, Phys. Rev. **133**, A1630 (1964); J. A. Switendick, A. C. Gossard, and V. Jaccarino, *ibid.* **136**, A1119 (1964); R. Kubo and Y. Obata, J. Phys. Soc. Jpn. **11**, 547 (1956); Y. Obata, *ibid.* **18**, 1020 (1964).
[19]W. Klemm and H. Fricke, Z. Anorg. Allg. Chem. **282**, 162 (1955).
[20]S. N. Ray, T. P. Das, J. Andriessen, and P. C. Schmidt, Bull. Am. Phys. Soc. **23**, 287 (1978).
[21]T. Loucks, *Augmented Plane Wave Method* (Benjamin, New York, 1967); J. O. Dimmock, in *Solid State Physics,* edited by H. Ehrenreich, F. Seitz and D. Turnbull (Academic, New York, 1971), Vol. 26, p. 104.
[22]J. C. Slater, J. Chem. Phys. **57**, 2389 (1972).
[23]J. F. Janak, Phys. Rev. B **9**, 3985 (1974).
[24]A. H. MacDonald and S. H. Vosko, J. Phys. C **12**, 2977 (1979).
[25]D. D. Koelling and B. N. Harmon, J. Phys. C **10**, 3107 (1977).
[26]J. C. Slater, Phys. Rev. **81**, 385 (1951).
[27]L. Hedin and S. Lundqvist, J. Phys. (Paris) Colloq. **33**, C3-73 (1972).
[28]U. von Barth and L. Hedin, J. Phys. C **5**, 1629 (1972).
[29]S. H. Vosko, L. Wolk, and M. Nusair, Can. J. Phys. **58**, 1200 (1980).
[30]J. C. Slater and P. de Cicco, Massachusetts Institute of Technology Solid State Theory Group Report No. 50, 1964 (unpublished).
[31]F. Hund, Z. Phys. **94**, 11 (1935); M. P. Tosi, in Solid State Physics, edited by H. Ehrenreich, F. Seitz, and D. Turnbull (Academic, New York, 1964), Vol. 16, p. 1.
[32]U. Takahasi and Y. Sakamoto, J. Sci. Hiroshima Univ. **A24**, 117 (1960); Y. Sakamoto, J. Chem. Phys. **30**, 337 (1959); F. Y. Hajj, J. Phys. C **6**, 2757 (1973).
[33]S. Asano and J. Yamashita, J. Phys. Soc. Jpn. **30**, 667 (1971).
[34]E. M. Rose, *Relativistic Electron Theory* (Wiley, New York, 1961).
[35]P. C. Schmidt, Ber. Bunsenges. Phys. Chem. **79**, 1064 (1975).
[36]S. D. Silverstein, Phys. Rev. **130**, 912 (1963); A. Narath and H. Weaver, *ibid.* **175**, 373 (1968).
[37]S. D. Mahanti and T. P. Das, Phys. Rev. **183**, 674 (1969).

[38]G. Lehmann and M. Taut, Phys. Status Solidi B **54**, 469 (1972).
[39]L. F. Mattheiss, J. H. Wood, and A. C. Switendick, Methods Comput. Phys. **8**, 64 (1968).
[40]T. Asada, T. Jarlborg, and A. J. Freeman, Phys. Rev. B **24**, 510 (1981).
[41]J. B. Conklin, Jr., L. E. Johnson, and G. W. Pratt, Jr., Phys. Rev. **137**, A1282 (1965).
[42]J. Friedel, Adv. Phys. **3**, 446 (1954).
[43]J. Robertson, Solid State Commun. **47**, 899 (1983).
[44]P. T. Bailey, Phys. Rev. **170**, 723 (1968).
[45]L. Tterlikkis, S. D. Mahanti, and T. D. Das, Phys. Rev. **178**, 630 (1969).
[46]H. E. Schone and W. D. Knight, Acta Metall. **11**, 179 (1963).
[47]K. Kishio and J. O. Brittain, J. Phys. Chem. Solids **40**, 933 (1979).
[48]M. L. Huggins, Phys. Rev. **28**, 1086 (1926); L. Pauling and M. L. Huggins, Z. Kristallogr. **87**, 205 (1934).
[49]V. M. Goldschmidt, Z. Elektrochem. **34**, 453 (1929).